XLI CILAMCE
XLI Ibero-Latin American Congress on Computational Methods in Engineering
16-19 November, 2020 FOZ DO IGUAÇU PARANÁ – BRAZIL

L-BFGS BASED LEAST-SQUARES REVERSE TIME MIGRATION FOR REFLECTIVITY IMAGING

Kristian D. T. Bautista[1], Franciane C. Peters[1], Raphael V. M. de Souza [1] Webe J. Mansur [1]

[1]*LAMEMO/COPPE/UFRJ*
Cidade Universitária, 21941-596, Rio de Janeiro, Brazil
kristian.torres13@coc.ufrj.br

Abstract. Assuming kinematic accuracy on the migration velocity model, seismic least-squares migration seeks to overcome the drawbacks of traditional migration algorithms by approximating the inverse imaging operator within a linear inversion framework. In this paper, we combine reverse-time migration and the L-BFGS optimization method to iteratively reconstruct the true subsurface reflectivity model from seismic reflection measurements. In each iteration, the initial model is first demigrated using the Born approximation of the acoustic wave equation to generate the predicted seismic data. Then, the reflectivity is updated by minimizing the least-squares misfit function in the data domain. Furthermore, to speed up the convergence of the inversion algorithm, we preconditioned the gradient by the illumination compensation operator. Numerical examples demonstrate that, even in the presence of salt bodies, the inverse operator of the imaging problem can be used to obtain improved migrated sections with reduced artifacts, better resolution, and reflectors with more balanced amplitudes.

Keywords: LSRTM, L-BFGS, Seismic Inversion, Wave equation

1 Introduction

To recover the true distribution of subsurface reflectivity, the seismic imaging process attempts to map the signal from the data domain to the reflectivity domain, which requires the action of an inverse operator. However, conventional migration techniques employ adjoint operators and imaging conditions to stabilize the migration of defective seismic data over a previously estimated background velocity distribution. These simplifications, along with limited bandwidth sources, under-sampled acquisition geometries, poor illumination and strong contrasts in the velocity model, generate artifacts that decrease the quality of the final image.

Least squares migration (LSM) seeks to overcome these drawbacks by approximating the exact inverse operator with a generalized inverse operator in the framework of a linear least squares problem. Different studies have shown its potential in reducing migration artifacts, removing acquisition marks, compensating for illumination, and increasing the resolution of seismic sections (Wang et al. [1], Nemeth et al. [2]).

To ensure good convergence rates, LSM could use fast linear inverse solvers (e.g. the linear conjugate gradient method), which require that the demigration and migration engines form an exact forward/adjoint operator pair, enabling the calculation of an optimal descent direction and the analytical step-length (Ji [3]). In practice, however, it is difficult to attain exact adjointness when computational subroutines imitate the action of matrix operators on the reflectivity model, due to memory constraints. Moreover, if the demigration and migration subroutines do not pass the dot product test (Claerbout [4]), convergence may be compromised. To circumvent this condition, it is convenient to calculate the step-length with a numerical line search strategy that guarantees the robustness of the optimization routines at each iteration by enforcing the sufficient decrease and curvature conditions (Nocedal and Wright [5]). Additionally, the performance of the LSM algorithm may also benefit from second-order optimization routines, which take into account the curvature of the objective function to scale the descent direction, providing a superlinear convergence rate.

Recent works have proposed LSM based on quasi-Newton algorithms. For example, Wu et al. [6] introduced a combination of the limited-memory Broyden–Fletcher–Goldfarb–Shanno method (L-BFGS) with least-squares pre-stack Kirchoff depth migration. In this work, we focus on extending the implementation of LSRTM under the L-BFGS method for pre-stack seismic data. Additionally, we show how including the illumination compensation as a preconditioning term helps to optimize the inversion process.

2 Theory

2.1 Conventional LSRTM

The first-order Born approximation of the two-way wave equation establishes a linear relation between the subsurface reflectivity model and the scattered seismic wavefield. Under such approximation, the solution of the following system of equations describes the LSRTM forward problem for the constant density acoustic wave equation:

$$\begin{cases} \left(s_0^2(\mathbf{x})\dfrac{\partial^2}{\partial t^2} - \nabla^2\right) u_0(\mathbf{x},t) = f\,(t)\,\delta\,(\mathbf{x}-\mathbf{x}_f) \\ \left(s_0^2(\mathbf{x})\dfrac{\partial^2}{\partial t^2} - \nabla^2\right) \delta u(\mathbf{x},t) = -2s_0(\mathbf{x})\delta s(\mathbf{x})\dfrac{\partial^2 u_0(\mathbf{x},t)}{\partial t^2} \end{cases}, \tag{1}$$

where s_0 and δs are, respectively, the background and perturbation slowness field, ∇^2 denotes the Laplacian operator, u_0 is the background wavefield associated with the point source $f(t)$ located at $\mathbf{x}_f$, and δu is the scattered wavefield with only primary reflection components.

Since δu is scaled linearly by the product between the second derivative of the mainly down-going background wavefield and the terms associated with the slowness field, the forward modeling can also be expressed in matrix-vector notation as:

$$\mathbf{d} = \mathbf{L}\mathbf{m}, \tag{2}$$

where $\mathbf{d}$ is the modeled scattered seismic data recorded at the receiver locations, $\mathbf{L}$ is the kernel of the PDE system in eq. (1) (also known as the demigration operator), and $\mathbf{m} = -2s_0(\mathbf{x})\delta s(\mathbf{x})$ represents the true reflectivity model as a function of the slowness perturbation.

The reverse time migration of seismic data (RTM) is considered to be the adjoint of the demigration operator. Therefore, the relation

$$\mathbf{m}_{\text{mig}} = \mathbf{L}^{\text{T}}\mathbf{d}, \tag{3}$$

in which $\mathbf{m}_{\text{mig}}$ represents the standard RTM image, gives a rough approximation of the true reflectivity. Usually, eq. (3) is computed through the conventional zero-lag cross-correlation imaging condition (Whitmore [7]).

The LSRTM inverse problem is formulated by substituting eq. (2) into eq. (3) and solving for the true reflectivity model:

$$\begin{aligned} \mathbf{m} &= (\mathbf{L}^{\text{T}}\mathbf{L})^{-1}\mathbf{m}_{\text{mig}}, \\ \mathbf{m} &= (\mathbf{L}^{\text{T}}\mathbf{L})^{-1}\mathbf{L}^{\text{T}}\mathbf{d}, \end{aligned} \tag{4}$$

which also represents the system of normal equations. In eq. (4), the Hessian matrix $\mathbf{H} = \mathbf{L}^{\text{T}}\mathbf{L}$ is too computationally expensive to store or invert directly. Thus, we estimate its inverse iteratively by minimizing the quadratic misfit function $E(\mathbf{m})$, defined as the least-squares norm of the residual:

$$\min_{\mathbf{m}\in\mathbb{R}^n} E(\mathbf{m}) = \frac{1}{2}\|\mathbf{L}\mathbf{m} - \mathbf{d}_{\text{obs}}\|_2^2, \tag{5}$$

where $\mathbf{d}_{\text{obs}}$ stands for the pre-stack observed seismic data. Finally, the iterative process is performed following the recursion

$$\mathbf{m}_{k+1} = \mathbf{m}_k + \alpha_k \Delta\mathbf{m}_k, \tag{6}$$

where α_k denotes the step length at each iteration k, and $\Delta\mathbf{m}_k$ is the descent direction, which can be found using the L-BFGS algorithm (Nocedal and Wright [5]).

2.2 L-BFGS method

For the quasi-Newton methods, the descent direction of the iterative inversion is defined as:

$$\Delta\mathbf{m}_k = -\mathbf{B}_k\mathbf{g}_k, \tag{7}$$

where $\mathbf{g}_k$ is the gradient of the misfit function, calculated through the migration of the data residual:

$$\mathbf{g}_k = \mathbf{L}^{\mathrm{T}}(\mathbf{L}\mathbf{m}_k - \mathbf{d}_{\mathrm{obs}}), \tag{8}$$

and $\mathbf{B}_k \approx \mathbf{H}^{-1}$ is an approximate Hessian inverse operator. Among the family of quasi-Newton methods, the L-BFGS is the most popular algorithm due to its efficiency, specially in problems with large number of variables. This method recursively calculates the product $\mathbf{B}_k\mathbf{g}_k$ with a limited number l of gradient and model vector pairs without the need to explicitly form the matrix $\mathbf{B}_k$. Starting from an initially estimated positive definite matrix $\mathbf{B}^0$, and defining $\mathbf{y}_k = \mathbf{g}_{k+1} - \mathbf{g}_k$ and $\mathbf{s}_k = \mathbf{m}_{k+1} - \mathbf{m}_k$, the descent direction for the kth iteration is calculated as follows (Nocedal and Wright [5]):

Algorithm 1: L-BFGS calculation of descent direction $\Delta\mathbf{m}_k = \mathbf{B}_k\mathbf{g}_k$.

Input: $\mathbf{g}_k$ e $\mathbf{B}_k^0$
begin
  Define $\mathbf{q} = \mathbf{g}_k$;
  for *i=k-1,...,k-l* **do**
    $\rho_i = \frac{1}{\mathbf{y}_i^{\mathrm{T}}\mathbf{s}_i}$
    $v_i = \rho_i \mathbf{s}_i^{\mathrm{T}}\mathbf{q}$
    $\mathbf{q} = \mathbf{q} - v_i\mathbf{y}_i$
  end for
  $\Delta\mathbf{m}_k = \mathbf{B}_k^0\mathbf{q}$
  for *i=k-1,...,k-l* **do**
    $\beta = \rho_i \mathbf{y}_i^{\mathrm{T}}\Delta\mathbf{m}_k$
    $\Delta\mathbf{m}_k = \Delta\mathbf{m}_k + \mathbf{s}_i(v_i - \beta)$
  end for
end

When Algorithm 1 is applied to reflectivity imaging, we choose $\mathbf{B}^0$ as any approximation of the inverse of the diagonal Hessian (Dai et al. [8]). In this work, we set $\mathbf{B}^0$ as the illumination compensation proposed by Plessix and Mulder [9] because it is a diagonal matrix with positive elements and it is also cheap to compute since we only require the background wavefield propagation, which is already available during the forward modeling step. Furthermore, since LSM is a linear inverse problem, neither the background velocity model nor $\mathbf{B}^0$ change during the iterative process.

3 Numerical experiments

In this section we present the results obtained by applying our pre-stack LSRTM algorithm on two modified versions of the Sigsbee2a synthetic model (Paffenholz et al. [10]). For both datasets we simulate a pre-processing step where the direct wave, the refracted waves and the surface-related multiple are removed from the pre-stack seismic gathers, since those events cannot be predicted by the demigration operator. However, in order to avoid the inverse crime, we keep the internal multiples. A Ricker wavelet with a peak frequency of 20 Hz is employed as the source function and it is assumed as known during the inversion. The two models are discretized on a regular finite difference grid with a gridpoint spacing of 5 m. The number of gradients stored for computing the L-BFGS approximation is set to $l = 5$. Below, the LSRTM results are compared with the RTM images.

3.1 Diffracting points under a salt body

The first experiment consists of imaging 9 diffracting points located near the bottom of a region with a smoothly varying velocity distribution and a high-velocity basement layer, as shown in Fig. 1. The model also contains a salt body. Only the diffracting points are considered as the reflectivity perturbation to be imagined. In other words, the background velocity model is the same as the true model without the presence of the diffracting points. This configuration was chosen to evaluate the imaging performance of LSRTM under the preconditioned L-BFGS method for subsurface targets near and under salt structures with complex geometries, where illumination is limited. In addition, the diffracting points are fundamental elements in seismic imaging as they can be employed to construct any complex reflector (Claerbout [4]). They also give a direct measure of image quality, particularly resolution.

Least-squares migration has the potential for efficiently reconstructing the reflectivity model when applied to incomplete data and poorly sampled shooting acquisitions, as it helps to reduce acquisition artifacts in a natural way (Nemeth et al. [2]). For this reason, in this test, we set a fixed-spread geometry with 500 receivers buried at a depth of 10 m, but only simulate 11 shots to emulate a seismic acquisition with poor source coverage.

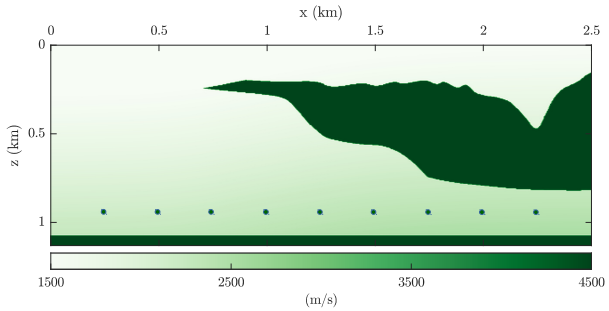

Figure 1. Velocity distribution for the diffracting points experiment.

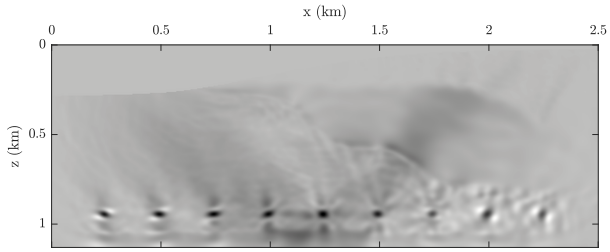

Figure 2. RTM image.

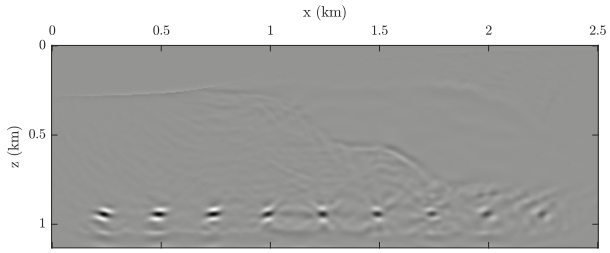

Figure 3. RTM result after the implementation of a Laplacian filter.

Figure 2 shows the result of the conventional RTM imaging. The synthetic data used for the imaging step only contains the up-going seismic wavefield produced by the diffracting points, since the other recorded events in the original seismograms are canceled by the difference between the background wavefield and the observed data during the pre-processing step, as shown in Fig. 6.c. Overall, the diffracting points are poorly imagined, the most affected being those positioned in the lower right part of the model, where the illumination is limited. The points on the left part of the image are tilted due to the presence of the salt body, that deflects the incident waves on the right side of the model, making the illumination of this region asymmetrical. The points located at the center are best imaged and most focused because the high-velocity basement layer produces the full internal reflection effect for the sources on the left side of the model. Evidence of this phenomenon is the presence of the V-shaped low-frequency artifact in the middle of the model, corresponding to the migration operator associated with the reflected waves.

Additionally, it can be noticed that the image is contaminated with low-frequency, high amplitude noise, produced by the high-velocity contrast in the model. We implement a Laplacian filter to remove such artifacts, and the result is shown in Fig. 3. Note that low-frequency noise is reduced almost completely, but high-frequency artifacts still remain in the image, and the diffracting points continue to have a blurred appearance and unbalanced, asymmetrical amplitudes.

The result obtained by the LSRTM inversion are shown in Fig. 4.a and Fig. 4.b, for 20 iterations (preliminary result) and 100 iterations (final result), respectively. Additionally, Fig. 5 shows the evolution of the objective function in relation to the number of iterations.

Comparing both results in Fig. 4 is evident that later iterations contribute to improve the focusing of the diffracting points and to reduce the presence of elements that are not part of true reflectivity model such as the migration artifacts related to the salt body.

Finally, Fig. 6 shows how the $\mathbf{L}$ operator applied to the inverted reflectivity model produces reflections that are much closer to the observed data, compared to the synthetic data obtained from the original RTM image.

3.2 Re-sampled Sigsbee2a model

The second test consist in applying the LSRTM with a precondtioned L-BFGS algorithm to a re-sampled version of the original Sigsbee2a model in a grid with 1200×400 points. The observed data are generated using

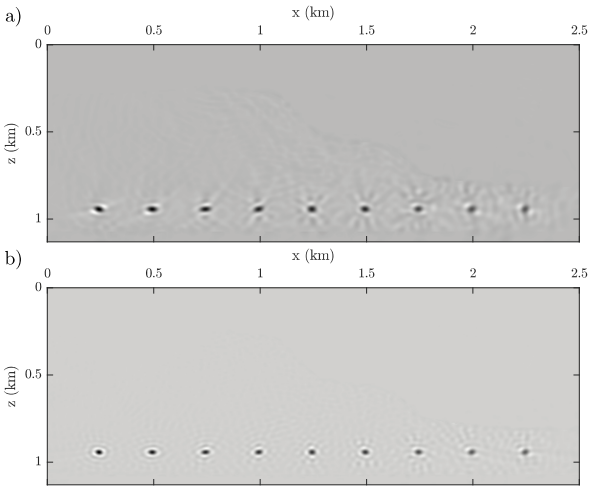

Figure 4. LSRTM inversion results. a) 20 iterations. b) 100 iterations.

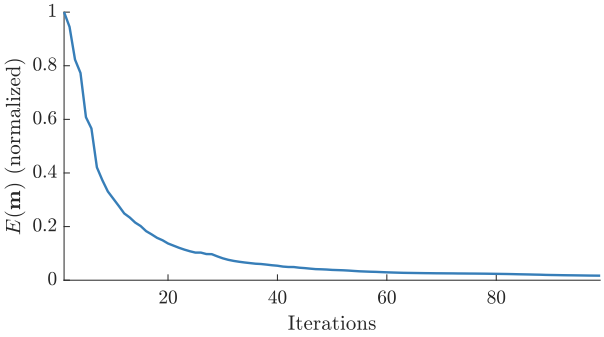

Figure 5. Evolution of the LSRTM inversion for the 9 diffracting points model.

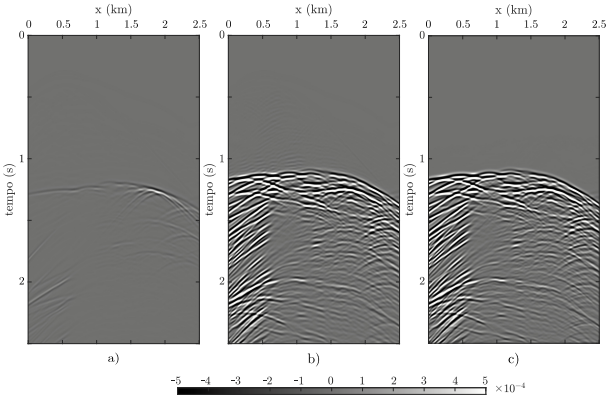

Figure 6. Comparison between synthetic seismograms calculated from Born modeling for a shot gather located at x = 625 m. a) Demigrated data from initial RTM image. b) Demigrated data from LSRTM result (100th iteration). c) Pre-stacked observed data.

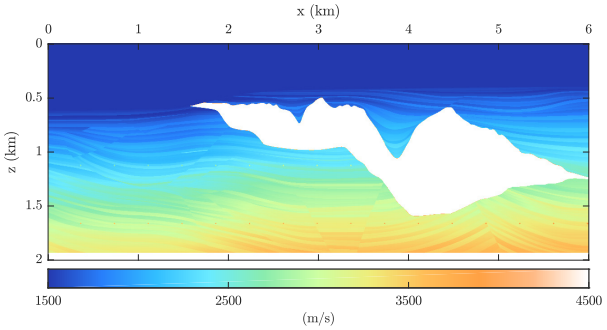

Figure 7. True velocity distribution of the resampled Sigsbee2a model.

the velocity model shown in Fig. 7. The background velocity field used for migration was obtained by applying a smoothed gaussian smoothing filter on the real model. The true reflectivity model is shown in Fig. 8.

Initially, a conventional RTM migration was performed, simulating an acquisition with 601 shots separated at 10 m intervals, and 1200 fixed receivers buried at a depth of 10 m. The result in Fig. 9 shows that the reflectors are contaminated by low-frequency artifacts, especially near the salt body. Figure 10 illustrates the migrated section after applying a Laplacian filter. Note that some of the artifacts still persist after filtering, as well as lack of reflector continuity.

The computational cost involved in multiple iterations of LSRTM is significantly higher than that of RTM. Consequently, we only use a subset of 61 shots for this numerical test. The LSRTM image obtained as a result of the iterative process is shown in Fig. 11, after applying a Laplacian filter. Compared to the conventional RTM section, this result has fewer artifacts. For example, the large amplitudes at the top of the salt are dramatically decreased. In addition, the edges of the image are better reconstructed, indicating that the inversion can compensate for model regions with low signal multiplicity. This is also evident in the pre-salt area on the lower right side of the model where reflectors that had not been imaged by the RTM operator are recovered despite the lack of illumination. It is notorious that most reflectors have better continuity and more balanced amplitudes. Furthermore, it was possible to obtain a higher resolution migrated section using only a subset of the total sources employed in the generation of the initial RTM section (approximately one-tenth of the total shots).

However, some high-frequency artifacts with no geological meaning are still present in the inverted image. As an example, it can be pointed out the left region under the salt flank at approximately 1 km of depth, where vertical ringing artifacts cut the flat reflectors. Clearly, LSRTM could be benefit from a smoothed regularization term to reduce these unwanted effects related to data over-fitting.

Finally, Fig. 12 shows the evolution of the objective function for the LSRTM inversion with and without the presence of the illumination compensation as the preconditioned term. For the L-BFGS without preconditioning, $\mathbf{B}^0$ was set as the identity matrix. It can be seen that the preconditioned L-BFGS offers better results at any stage of the inversion and also reaches the local minima in fewer iterations, compared to the conventional L-BFGS.

4 Conclusions

In this work, we showed that it is possible to obtain improved resolution reflectivity distributions through the L-BFGS algorithm, avoiding convergence problems associated with pseudo adjoint operators.

Regarding the numerical experiments performed in LSRTM inversion, it was possible to obtain sections with significant improvements in the imaging of seismic horizons, especially in regions near the salt body in modified versions of the Sigsbee2a model. Even though there is a considerable gain in amplitude balancing, focusing and low-frequency noise reduction, it is concluded that it is necessary to incorporate smoothing techniques to reduce high-frequency artifacts.

Acknowledgements

The authors would like to thank the Coordenação de Aperfeiçoamento de Pessoal de Nível Superior-Brasil (CAPES) - Finance Code 001, Faperj (203.234/2016, 210.210/2016, 201.453/2014, 203.021/2017, 200.262/2015), Petrobras (CENPES - 014987) and The Society of Exploration Geophysicists (SEG) Scholarship's program.

References

[1] Wang, P., Huang, S., & Wang, M., 2017. Improved subsalt images with least-squares reverse time migration. *Interpretation*, vol. 5, n. 3, pp. SN25–SN32.

[2] Nemeth, T., Wu, C., & Schuster, G. T., 1999. Least-squares migration of incomplete reflection data. *Geophysics*, vol. 64, n. 1, pp. 208–221.

[3] Ji, J., 2009. An exact adjoint operation pair in time extrapolation and its application in least-squares reverse-time migration. *Geophysics*, vol. 74, n. 5, pp. H27–H33.

[4] Claerbout, J. F., 1992. *Earth soundings analysis: Processing versus inversion*, volume 6. Blackwell Scientific Publications, Ltd.

[5] Nocedal, J. & Wright, S., 2006. *Numerical optimization*. Springer Science & Business Media.

[6] Wu, S., Wang, Y., Zheng, Y., & Chang, X., 2015. Limited-memory BFGS based least-squares pre-stack Kirchhoff depth migration. *Geophysical Journal International*, vol. 202, n. 2, pp. 738–747.

[7] Whitmore, N. D., 2005. *Iterative depth migration by backward time propagation*, pp. 382–385.

[8] Dai, W., Fowler, P., & Schuster, G. T., 2012. Multi-source least-squares reverse time migration. *Geophysical Prospecting*, vol. 60, n. 4, pp. 681–695.

[9] Plessix, R.-E. & Mulder, W. A., 2004. Frequency-domain finite-difference amplitude-preserving migration. *Geophysical Journal International*, vol. 157, n. 3, pp. 975–987.

[10] Paffenholz, J., McLain, B., Zaske, J., & Keliher, P. J., 2002. Subsalt multiple attenuation and imaging: Observations from the Sigsbee2B synthetic dataset. In *SEG Technical Program Expanded Abstracts 2002*, pp. 2122–2125. Society of Exploration Geophysicists.

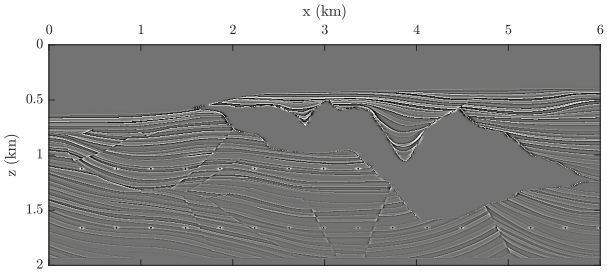

Figure 8. True reflectivity of the resampled Sigsbee2 model.

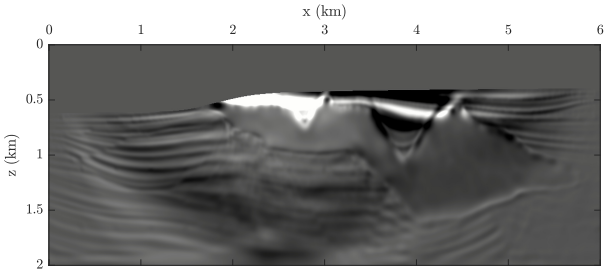

Figure 9. RTM section obtained with the original dataset (601 shots).

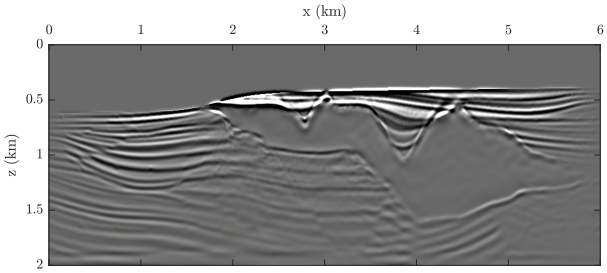

Figure 10. Filtered RTM section.

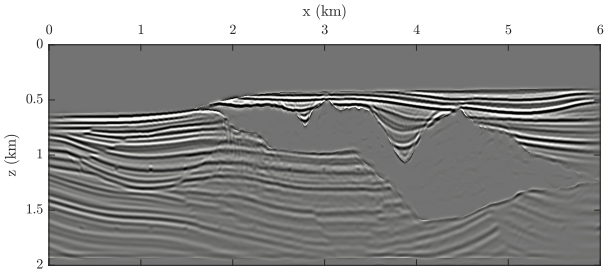

Figure 11. LSRTM filtered section after 25 iterations. This result should be compared to the RTM image in Fig. 10

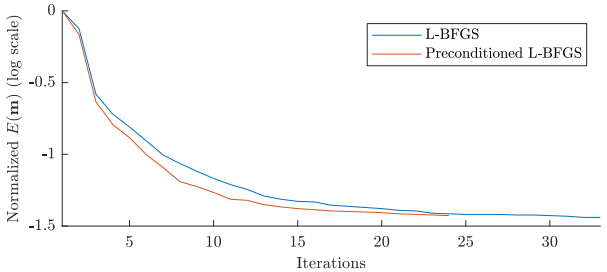

Figure 12. The curves of the normalized objective function over iterations.